Masking of the Fc region in human IgG4 by constrained X-ray scattering modelling: implications for antibody function and therapy

Yuki Abe, Jayesh Gor, Daniel G Bracewell, Stephen J Perkins, Paul A. Dalby

Masking of the Fc region in human IgG4 by constrained X-ray scattering modelling: implications for antibody function and therapy

Yuki Abe[*], Jayesh Gor[†], Daniel G. Bracewell[*], Stephen J. Perkins[‡†] and Paul A. Dalby[‡]

[*]Department of Biochemical Engineering,
Division of Engineering
Roberts Building,
University College London,
Gower Street,
London WC1E 6BT, U.K.

[†]Department of Structural and Molecular Biology,
Division of Biosciences
Darwin Building,
University College London,
Gower Street,
London WC1E 6BT, U.K.

Running Title: Solution structure of IgG4

Keywords: Antibody; analytical ultracentrifugation; constrained modelling; X-ray scattering.

Abbreviations: IgG, immunoglobulin G; IgG4, IgG subclass 4.

‡ Authors to whom correspondence and requests for reprints should be addressed (SJP: Tel: 020-7679-7048; Fax: 020-7679-7193; email s.perkins@medsch.ucl.ac.uk) (PAD: Tel: 020-7679-2962; Fax: 020-7679-3540; Email: p.dalby@ucl.ac.uk). Editorial correspondence should be sent to SJP.

The text consists of 30 pages (including 7 Figures and 2 Tables), plus a Supplementary Material section with 3 Figures and 1 Table.

SYNOPSIS

Of the four human IgG antibody subclasses IgG1-IgG4, IgG4 is of interest in that this does not activate complement and exhibits atypical self-association including the formation of bispecific antibodies. The solution structures of antibodies are critical to understand function and therapeutic applications. Thus IgG4 was studied by synchrotron X-ray scattering. The Guinier X-ray radius of gyration R_G increased from 5.0 nm to 5.1 nm with increase of concentration. The distance distribution function *P(r)* revealed a single peak at 0.3 mg/ml, which are resolved into two peaks that shifted to smaller *r* values at 1.3 mg/ml, even though the maximum dimension of IgG4 was unchanged at 17 nm. This indicated a small concentration dependence of the IgG4 solution structure. By analytical ultracentrifugation no concentration dependence in the sedimentation coefficient of 6.4 S was observed. Constrained scattering modelling resulted in solution structural determinations that showed that IgG4 has an asymmetric solution structure in which one Fab-Fc pair is closer together than the other pair, and the accessibility of one side of the Fc region is masked by the Fab regions. The averaged distances between the two Fab-Fc pairs change by 1-2 nm with change in IgG4 concentration. The averaged conformation of the Fab regions appear able to hinder complement C1q binding to the Fc region and the self-association of IgG4 through the Fc region. These results clarify IgG4 function and provide a starting point to investigate antibody stability.

INTRODUCTION

The average serum concentrations of the four human IgG subclasses (IgG1, IgG2, IgG3 and IgG4) are 8 mg/ml, 4 mg/ml, 0.8 mg/ml and 0.4 mg/ml respectively [1]. The four subclasses IgG1-IgG4 primarily differ at their hinges that connect the Fab and Fc regions (Figure 1) [1,2]. While human IgG2 and IgG4 both have hinges of 12 residues in length, human IgG1 and IgG3 have hinges of length 15 or 62 residues respectively. The hinge is comprised of upper, middle and lower sections. The upper hinge connects the Fab region to the Cys-rich middle hinge, while the lower hinge connects the Fc region to the middle hinge. The genetic hinge corresponds to the upper and middle hinges, while the lower hinge is encoded by the C_H2 exon, and the three hinge sections in the four subclasses differ in sizes. The subclasses relate to different activities, in which IgG4 with the shortest upper hinge is unable to activate complement, while IgG1 and IgG3 are very effective, and IgG2 is only effective at high concentration [2]. IgG4 also shows poorer binding to Fc receptors [1]. Additionally IgG4 differs in being monovalent, when it can bind to two different antigens through two different Fab regions [3,4]. A mutation from proline to serine in the middle hinge shifts the disulphide bond equilibrium in IgG4 and allows the ready exchange of pairs of heavy and light chains to form bispecific antibodies [3]. Such exchange may play an important role in the *in vivo* function of IgG4. The 25-75% loss of this disulphide bond potentially leads to greater conformational freedom of the IgG4 hinge region that may be expected to vary with solution conditions. In the pharmaceutical industry, even though antibodies comprise one-third of drugs, and IgG1 monoclonal antibodies are the most commonly exploited subclass, IgG4 is the basis of several successfully approved biopharmaceuticals for reason of its lack of inflammatory reaction in treatments, including those for myeloid leukaemia (Gemtuzumab ozogamicin), paroxysmal nocturnal hemoglobinemia (Eculizumab), and multiple sclerosis (Natalizumab) [5,6].

Structural studies of the human IgG subclasses are important for functional and therapeutic applications. Knowledge of the relative positions of the Fab and Fc regions in solution is important for both antigen and receptor interactions [1,2,7,8]. In this context, protein crystal structures of intact IgG antibodies are relatively few, and correspond to single hinge conformations that are trapped within the crystallographic unit cell [9-12]. Likewise a knowledge of antibody aggregation behaviour during manufacture, shipping and storage is critical to minimising unwanted immunogenic effects *in vivo* [13,14]. This understanding is based largely on experimental studies of solution parameters such as the temperature and process environment [15,16]. Therefore, antibody solution structures in solution are required under a wide range of conditions. So far, such structure determinations of IgG antibodies have been restricted to relatively few examples. Neutron scattering structures for the bovine IgG1 and IgG2 subclasses were determined by constrained modelling based on Fab and Fc crystal structures [17]. Low resolution solution conformations for human IgG4 were obtained by hydrodynamic ellipse and bead modelling of ultracentrifugation data [18-21]. Other approaches have included electron microscopy *in vacuo* which showed that IgG4 demonstrated less hinge flexibility compared to IgG1 or IgG3, and was less able to form bivalent ring dimers [22].

Here, we describe solution structure determinations for IgG4 by X-ray scattering and analytical ultracentrifugation combined with constrained modelling based on the human IgG1 crystal structure [10]. This combination of methods yields more detailed antibody solution structures than those from hydrodynamic bead modelling alone [23,24]. By this, solution structures have been determined for pentameric human IgM, human IgA1 and IgA2, human

IgD, and a murine Crry-Fc chimaeric therapeutic antibody [17,25-29]. Structures are archived in the Protein Data Bank. Because X-ray scattering data can now be measured within seconds [30], it is possible to follow protein conformations as a function of different solution conditions [31]. Here, in combination with analytical ultracentrifugation to establish the monodispersity of IgG4 [32], we show that the averaged solution structure of IgG4 possesses semi-extended hinges and exhibits a detectable conformational dependence on concentration. We show that the Fab regions mask one side of the Fc region in IgG4, unlike the arrangement seen in the IgG1 crystal structure, and this may perturb the functional ability of IgG4 to bind complement and to self-associate. .

EXPERIMENTAL

Purification and composition of IgG4

A human-mouse chimera IgG4 B72.3 that binds to tumour cells was generously supplied by Dr J. Davies at Lonza Biologics (https://www.lonza.com/group/en.html). IgG4 was further purified by gel filtration chromatography using a Superose 6/300 column (GE Healthcare) to remove large non-specific aggregates, then dialysed extensively at 4 °C against phosphate buffered saline (PBS) (10.6 mM sodium phosphate, 1.5 mM potassium phosphate, 138 mM NaCl, 2.7 mM KCl at pH 7.4). In this IgG4, the heavy and light chain amino acid sequences of the human-mouse chimera Fab region are reported in its PDB structure file (PDB code 1bbj: [33]), and included its human κ light chain. In this PDB file, the C-terminal Cys residue is truncated in the C_L sequence (Supplementary Figure 1); this is expected to be bridged with Cys148 in the C_H1 domain. The engineered variable domains V_H and V_L originated from a mouse antibody, whereas the remaining sequence is from human IgG4. The C_H1 domain, hinge and Fc region sequences were taken from its Genbank sequence (accession code AAG00912). The carbohydrate composition was assumed to be similar to that for N-linked oligosaccharides in human IgG, in which each of the Asn314 residues in the Fc region (Figure 1) contain a complex-type oligosaccharide with a $Man_3GlcNAc_2$ core and two NeuNAc.Gal.GlcNAc antennae. This resulted in a IgG4 calculated molecular weight of 145.5 kDa, an unhydrated volume of 187.2 nm^3, a hydrated volume of 246.6 nm^3 (based on a hydration of 0.3g H_2O/g of glycoprotein and an electrostricted volume of 0.0245 nm^3 per bound water molecule), a partial specific volume ν of 0.728 ml/g, and an absorption coefficient at 280 nm (1%, 1 cm path length) of 14.7 [34]. The buffer density of PBS was taken as the default value of 1.00543 g/ml; this value was corroborated at 20°C using an Anton-Paar DMA5000 density meter to be 1.00526 g/ml.

Sedimentation velocity data for IgG4

Analytical ultracentrifugation data for IgG4 were obtained on two Beckman XL-I instruments equipped with AnTi50 and AnTi60 rotors. Sedimentation velocity data was acquired at 20°C at rotor speeds of 50,000 r.p.m. and 60,000 r.p.m. in two-sector cells with column heights of 12 mm. Sedimentation analysis was performed using direct boundary Lamm fits of up to 300 scans using SEDFIT (version 11.71) [35,36]. SEDFIT resulted in size-distribution analyses *c(s)*, the algorithm for which assumes that all species have the same frictional ratio f/f_o. The final SEDFIT analyses used a fixed resolution of 200 and optimised the *c(s)* fit by floating f/f_o and the baseline until the overall root mean square deviations and visual appearance of the fits were satisfactory. The percentage fraction of oligomers in the total loading concentration was derived using the *c(s)* integration function.

X-ray scattering data for IgG4

X-ray scattering data were obtained during one beam session in four-bunch mode at the European Synchrotron Radiation Facility (ESRF), Grenoble, France, operating with a ring energy of 6.0 GeV on the Beamline ID02 [37]. Storage ring currents ranged from 31 mA to 39 mA. Data were acquired using a recently installed fibre optically-coupled high sensitivity and dynamic range CCD detector (FReLoN). Together with a smaller beam stop and the use of a detector resolution of 512 × 512 pixels, this allowed a shorter sample-to-detector distance of 2.0 m to be used and resulted in higher signal-to-noise ratios [38]. IgG4 was studied at four concentrations between 0.3 mg/ml to 1.3 mg/ml, in which samples of volume 100 µl were measured in flow cells to reduce radiation damage by moving the sample continuously during beam exposure. Sets of ten time frames each, with frames of duration 0.1 sec or 0.2 sec each, were acquired in quadruplicate as a control of reproducibility. On-line

checks during data acquisition confirmed the absence of radiation damage, after which the ten frames were averaged. Other details including the data reduction procedure are described elsewhere [39]. A second X-ray beam session utilised IgG4 at 0.3 mg/ml only, which was used to verify the above data set, but not used here.

In a given solute-solvent contrast, the radius of gyration R_G is a measure of structural elongation if the internal inhomogeneity of scattering densities within the protein has no effect. Guinier analyses at low Q gives the R_G, and the forward scattering at zero angle $I(0)$ [40]:

$$\ln I(Q) = \ln I(0) - R_G^2\, Q^2/3.$$

This expression is valid in a $Q.R_G$ range up to 1.5. If the structure is elongated, the mean radius of gyration of cross-sectional structure R_{XS} and the mean cross-sectional intensity at zero angle $[I(Q)Q]_{Q\rightarrow 0}$ is obtained from:

$$\ln [I(Q)Q] = [I(Q)Q]_{Q\rightarrow 0} - R_{XS}^2 Q^2/2.$$

For immunoglobulins, the cross-sectional plot exhibits two regions, a steeper innermost one and a flatter outermost one [41], and the two analyses are identified by $R_{XS\text{-}1}$ and $R_{XS\text{-}2}$ respectively. The R_G and R_{XS} analyses were performed using an interactive PERL script program SCTPL7 (J. T. Eaton and S. J. Perkins, unpublished software) on Silicon Graphics OCTANE Workstations. Indirect transformation of the scattering data $I(Q)$ in reciprocal space into real space to give the distance distribution function $P(r)$ was carried out using the program GNOM [42]:

$$P(r) = \frac{1}{2\pi^2}\int_o^\infty I(Q)\, Qr \sin(Qr)\, dQ$$

$P(r)$ corresponds to the distribution of distances r between volume elements. This yields the maximum dimension of the macromolecule L and its most commonly occurring distance vector M in real space. For this, the X-ray $I(Q)$ curve utilised up to 246 data points in the Q range between 0.06 nm^{-1} and 1.75 nm^{-1}.

Debye scattering and sedimentation coefficient modelling of IgG4

The homology model for IgG4 was constructed from the crystal structures of Fab B72.3 and human IgG1 (PDB codes 1bbj, 1hzh) [11,33]. The Fab B72.3 crystal structure incorporated the IgG4 residues up to Val232. A homology model for IgG4 between residues Cys243-Leu462 was created using SWISS-MODEL software available at http://swissmodel.expasy.org/ [43]. There is a 94.1% sequence identity between the two sequences. The 9-residue peptide used for randomisation was 232-VESKYGPPC-243, in which the central seven residues that correspond to the upper hinge were conformationally randomised using molecular dynamics, and the outermost residues were anchor points used to superimpose the hinge onto the Fab and Fc regions in order to create the full IgG4 model. The 9-residue peptide was first created in an extended β-strand conformation. Following Method 2 used for human IgA1 [26], two libraries of 5,000 randomised hinge conformations were generated. The 9-residue peptides were constrained to be of minimum lengths either (i) between 2.2 nm to 3.1 nm, or (ii) between 3.1 to 3.15 nm, where the latter hinges were almost fully extended in length. A minimum hinge length was required in order to prevent the hinge adopting abnormally short structures. Each hinge in duplicate was used to join the two Fab and Fc regions to create 10,000 IgG4 models. The centre-of-mass of each Fab or Fc region is defined as the midpoint of the line joining the midpoint of the four α-carbon atoms in the disulphide bridges of the β-strands B and F (i) between the V_H and V_L domains, and (ii) between the C_H1 and C_L domains.

Each full IgG4 model was used to calculate its X-ray scattering curve for comparison with the four experimental IgG4 curves (Table 1) using Debye sphere models [44]. A cube side length of 0.536 nm in combination with a cutoff of 4 atoms was used to convert the atomic coordinates into Debye sphere models with 1189 spheres that corresponded to the unhydrated structure. Because hydration shells are visible by X-rays, a hydration shell corresponding to 0.3 g H_2O/ g protein was created using HYPRO [45], where the optimal total of hydrated spheres in the IgG4 model is 1566 (Table 1). The X-ray scattering curve *I(Q)* was calculated using the Debye equation adapted to spheres [44]. Details are given elsewhere [46]. Steric overlap between the Fab and Fc regions in the models was assessed using the number of spheres *N* in the models after grid transformation, where models showing less than 95% of the required total of 1566 spheres were discarded. Over 66% of the 10,000 models met this "absence of steric overlap" criterion Next, the X-ray R_G and $R_{XS\text{-}1}$ values were calculated from the modelled curves in the same *Q* ranges used for the experimental Guinier fits. This allowed for any approximations inherent in the use of the $Q.R_G$ fit range up to 1.5. Models that passed R_G and $R_{XS\text{-}1}$ filters of ± 5% were then ranked using a goodness-of-fit *R* factor defined by analogy with protein crystallography and based on the experimental curves in the Q range extending to1.8 nm^{-1} (Table 1). The distances *d1*, *d2* and *d3* were determined from the centres of mass of the Fab and Fc regions (excluding hydrogen atoms) using a script written in PYTHON. The three angles between the Fab and Fc regions were defined as the angle of intersection from the dot product between two vectors, also using a PYTHON script. Each vector was the long axis through each Fab or Fc region, where the axes were defined as the lines passing through the centres of gravity between each cluster of four Cys α-carbon atoms at the two ends of the Fab and Fc regions (one cluster at each end of each Fab or Fc region, corresponding to the conserved disulphide bridge in each immunoglobulin fold domain). Artwork was prepared using PYMOL software (http://www.pymol.org/).

Sedimentation coefficients $s^0_{20,w}$ were calculated directly from the hydrated Debye sphere models using the program HYDRO as a confirmation of the GENDIA analysis [47]. They were also calculated from the atomic coordinates in the HYDROPRO shell modelling program using the default value of 0.31 nm for the atomic element radius for all atoms to represent the hydration shell [48]. Previous applications of these calculations to antibodies are reviewed elsewhere [24,49].

Protein Data Bank accession number

The best-fit IgG4 α-carbon co-ordinate models have been deposited in the Protein Data Bank with the accession codes 3m7x (1.3 mg/ml), 3m7y (0.98 mg/ml), 3m7z (0.65 mg/ml) and 3m80 (0.30 mg/ml).

RESULTS

Purification and analytical ultracentrifugation of IgG4

A chimaeric mouse-human IgG4 antibody that possesses Ser245 and not Pro245 in its hinge (alternatives names: Ser228 in [2]; Ser331 in [20]; Ser241 in [21]) was used. In this, the mouse V_H and V_L domains are combined with the human C_L, C_H1, C_H2 and C_H3 domains (Figure 1). IgG4 was subjected to gel filtration to remove potential non-specific aggregates immediately prior to ultracentrifugation or scattering experiments. This eluted as a single peak with a trailing edge (Figure 2(a)). Purified IgG4 showed four bands on SDS-PAGE under non-reducing conditions. These indicate the observation of the intact IgG4 molecule (apparent molecular weight 190 kDa) together with separated pairs of disulphide-linked heavy-light chains (apparent molecular weight 90 kDa) and the individual heavy and light chains on their own (apparent molecular weights 60 kDa and 25 kDa) (Figure 2(b)). This is consistent with the presence of the two known isomeric forms of IgG4, one formed by interchain Cys-Cys bridges at Cys243 and Cys246, and the other lacking inter heavy-chain disulphides (Figure 1) [3,50]. Only heavy chains (apparent molecular weight 55 kDa) and light chains (apparent molecular weight 25 kDa) were observed in reducing conditions (Figure 2(c)). This purified IgG4 was found to be stable upon storage at 4°C for at least a month.

Sedimentation velocity experiments were performed as a check of monodispersity and for shape determinations. Runs were performed for IgG4 concentrations of 0.8 mg/ml (5.5 μM) and 1.6 mg/ml (11 μM) (Materials & Methods). The SEDFIT analysis of Figure 3 involved fits to as many as 150 scans, and the good agreement between the experimental boundary scans and fitted lines is clear. A regular sedimentation profile was observed, from which only a single peak was observed in the size distribution analysis *c(s)* in SEDFIT, with no other significant peaks observed. This single peak indicated that the IgG4 sample was monodisperse in solution, with no evidence for the separation of the two isomeric forms [50] or the existence of smaller species that had appeared in the harsh environment of the non-reducing SDS-PAGE analysis (Figure 2(b)). This agrees with previous reports of IgG4 stability [3]. This also agrees with the <1% dimers or oligomers seen for IgG4 when this was subjected to size-exclusion chromatography [53a]. The major peak was observed at $s_{20,w}$ values of 6.44 S. Since the sedimentation coefficient $s_{20,w}$ is a structural parameter of macromolecular elongation in solution, it can be compared with those for other related antibody molecules. These $s_{20,w}$ values are comparable with those reported for human IgA1 of 6.15-6.20 S [26], human IgA2 of 6.42-6.57 S [28], and human IgG4 of 6.20-6.80 S [18-21]. The calculation of the frictional coefficient ratio f/f_0 for IgG4 normalises the shape parameter by comparing this with that f_0 for a sphere of the same volume. From SEDFIT analyses, this was determined to be 1.37. From the value of 6.44 S and the composition, this ratio is 1.30 for IgG4, which is less than that of 1.56 for IgA1 and 1.53 for IgA2, and indicates that IgG4 is more compact in shape than IgA.

X-ray scattering of IgG4

The solution arrangement of the Fab and Fc fragments of IgG4 was analysed by synchrotron X-ray scattering. Data collection was carried out between 0.3-1.3 mg/ml (2 – 9 μM) at the ESRF, using time frame analyses to ensure the absence of radiation damage effects. Guinier analyses to measure the degree of elongation of IgG4 resulted in linear plots in three distinct regions of the *I(Q)* curves, as expected for antibodies, from which the R_G, R_{XS-1} and R_{XS-2} values were obtained within satisfactory $Q.R_G$ and $Q.R_{XS}$ limits (Figure 4). Only trace amounts of aggregates were present, as evidenced by the slight upturn in the

curves at the smallest Q values. These aggregates occurred before the Q range used for the Guinier analyses and did not perturb these analyses. The mean X-ray R_G value for IgG4 varied between 4.92 nm to 5.03 nm, with a mean of 4.99 nm (Table 1). On dilution, these increased slightly from 4.98 nm to 5.03 nm, then decreased to 4.92 nm. The $R_{XS\text{-}1}$ and $R_{XS\text{-}2}$ values were also similar in the concentration range, giving mean values of 2.56 nm and 1.40 nm respectively (Table 1). These R_G, $R_{XS\text{-}1}$ and $R_{XS\text{-}2}$ values are comparable with those for other antibodies such as those of IgA1 and IgA2, indicating that their general structural morphology in terms of structurally distinct Fab and Fc regions are similar. The anisotropy ratio R_G/R_O (where R_O is the R_G value of the sphere with the same volume as the hydrated glycoprotein) was calculated from the X-ray R_G values of IgG4 to be 1.63 to 1.67. Comparison of this ratio to that of 1.99 determined for human IgA1 and 1.66 for human IgA2 [26,28] showed that IgG4 is less elongated than IgA1, but is comparable in elongation with IgA2 in solution.

The distance distribution function $P(r)$ curve provides structural information in real space. From the $P(r)$ analysis, the R_G values were determined to range from 4.96 nm to 5.08 nm at the four concentrations, with a mean of 5.03 nm. These are within error of the mean R_G value of 4.99 nm from the Guinier analyses, and are therefore consistent with these (Table 1). The maximum length L of IgG4 was determined from the value of r when the $P(r)$ curve intersects $P(r) = 0$ to be 17.0 nm at all four concentrations (Table 1). The similarity of the $s_{20,w}$ R_G and L values showed that the overall shape of IgG4 remains unchanged as the concentration is varied. The peaks in the $P(r)$ curves correspond to the most frequently occurring interatomic distances within the structure. For IgG4, a single peak *M1* was obtained at an r value of 5.3 nm at 0.3 mg/ml; as the IgG4 concentration increases, a second peak *M2* becomes visible (Figure 5(a)). The two peaks show reproducible concentration dependences (Figure 5(b)). In the cases of other human antibodies, only a single peak *M1* was experimentally observed in the X-ray P(r) curve for human IgD, while two peaks *M1* and *M2* were observed for IgA1 and IgA2 [26,28,29]. The previous explanation for two $P(r)$ peaks for IgA1 and IgA2 was based on postulating relatively rigid hinge structures in IgA1 and IgA2 and their predominantly T-shaped structures. The single $P(r)$ peak for IgD was attributed to either the existence of either a different conformation in solution or the presence of sufficient hinge flexibility to result in multiple Fab and Fc arrangements, either of which would caused peak M2 to disappear. These explanations are corroborated by scattering curve simulations based on the static crystal structures of intact murine IgG1 and IgG2a (PDB codes 1igy and 1igt: [11,12]). The different Y-shaped or T-shaped Fab arrangements within IgG lead either to a single or double peak in their $P(r)$ curves respectively [28]. For IgG4, it is concluded that the movement of the *M1* and *M2* peaks with concentration reflect alterations in the Fab and Fc arrangement within its structure that do not affect its overall shape.

The similarity of the R_G values when set against the altered *M1* and *M2* values for IgG4 upon dilution implies that the scattering curve at 0.3 mg/ml is altered. Further inspection of the R_G, $R_{XS\text{-}1}$ and $R_{XS\text{-}2}$ values substantiated this. The single *M1* peak at 0.3 mg/ml was correlated with a slightly lower R_G value of 0.1 nm, an almost unchanged $R_{XS\text{-}1}$ value and a lower $R_{XS\text{-}2}$ value of about 0.2 nm when compared with the other three concentrations (Table 1).

Molecular modelling of IgG4 and its hinge region

In order to determine IgG4 solution structures that would account for the movement of the two peaks in the $P(r)$ curves, a starting model of IgG4 was constructed from the crystal structure of Fab B72.3 that corresponded to the mouse-human chimaera in use [33] and a

homology model for the Fc region that was constructed from the human IgG1 crystal structure [11]. The sequence identity between the IgG1 and IgG4 Fc regions was 94.1% (Supplementary Figure 1(f,g)). No residue insertions or deletions were required in the modelling, and the main template β-strand structures and locations of the highly conserved Cys residues were retained. A Ramachandran plot of the homology model using the structure validation program PROCHECK showed that all the residues fell within sterically acceptable values. There is a single oligosaccharide chain at Asn314 of IgG1 that is conserved at Asn314 in IgG4. The two complex-type oligosaccharide structures seen in the human IgG1 crystal structure with nine residues in each were retained unmodified in the IgG4 models. Both Asn314 residues are located at the top of the C_H2 domain in the Fc region, and the oligosaccharide chains point into the space between the two C_H2 domains.

The IgG4 hinge was modelled after examination of the IgG1 crystal structure. While the Fab region formally terminates at Ser234 (Figure 1; Supplementary Figure 1(d)), the end of the terminal β-strand G in this immunoglobulin domain is Arg231, after which there are no steric restraints on the tripeptide 232-VES-234. The full hinge itself is formally defined by the residues 233-ESKYGPPCPPSCPAPEFLGGP-255 [2], within which the Fc region formally starts at Leu252 (Figure 1; Supplementary Figure 1). Overall this hinge sequence is characterised by six proline residues and two Cys243 and Cys246 disulphide bridges in the numbering of Supplementary Figure 1. The latter are expected to tether the two hinge sequences to make these less flexible, especially between Cys243 and the Fc region. If the full hinge was conformationally randomised in the modelling, this would result in the separation of the two disulphide bridges. Accordingly the middle and lower hinge residues 243-CPSCPAPEFLGGP-255 were considered to be invariant and not modelled. It was concluded that IgG4 hinge variability would be best modelled by conformational sampling of a nine-residue peptide comprising the upper hinge 233-ESKYGPP-242 and the two terminal residues Val232 and Cys243 which were used for connections with the Fab and Fc regions (Supplementary Figure 1). Because this sequence 232-VESKYGPPC-243 is located asymmetrically in relation to the Fc structure, this meant that the IgG4 model does not have two-fold symmetry.

Randomised conformational search for IgG4 solution structures

A total of 10,000 IgG4 conformationally-randomised structures was assembled to model the IgG4 solution structure. Molecular dynamics resulted in a sufficiently wide range of orientations and translations of the two Fab and Fc fragments in IgG4 models for evaluation, while not necessarily satisfying the allowed regions in Ramachandran plots (Materials and Methods). In these, no account was taken of the two isomeric disulphide forms of IgG4 because these showed similar sedimentation properties (Figure 3) to indicate that they have similar solution structures. The simulation with 5,000 hinges of minimum length 3.1-3.15 nm to 3.15 nm generated 5,000 trial IgG4 structures with no two-fold axial symmetry about the Fc region. The resulting modelled scattering curves were compared with the experimental X-ray curves to give goodness-of-fit *R*-factors ranging between 2.0% to 27.0% (Table 1). When the *R*-factors were compared to their R_G values, the lowest *R*-factors correspond to models with R_G values close to the experimental R_G values (Supplementary Figure 2(a-d), upper row). The identification of a single minimum *R*-factor value in Supplementary Figure 2 showed that the modelling strategy was successful in generating a single family of possible solution structures for IgG4. A second simulation with 5,000 different IgG4 models with hinges of minimum length between 2.2 nm to 3.1 nm was also performed. The distributions of Supplementary Figure 2(a-d) (lower row) showed that fewer

models with larger R_G values were obtained, but nonetheless a similar minimum in *R*-factor values was obtained in all four cases. This indicated the reproducibility of the modelling, and also showed that extended hinges were required for good fits.

Filters based on the experimental scattering data were used with the 10,000 IgG4 models to reject unsatisfactory models and identify best-fit models.

(i) The ± 5% filter for steric overlap eliminated those models in which the Fab and Fc fragments and the hinge sterically overlapped as the result of inappropriate randomised hinge conformations generated by the simulations. A satisfactory IgG4 sphere model needed a minimum total number *N* of 1566 spheres in order to correspond to the composition-calculated volume of IgG4.

(ii) A ± 5% filter of the R_G values calculated from the models in the same Guinier Q ranges used for the four experimental X-ray R_G values of 4.92 nm to 5.03 nm identified those IgG4 models that fitted the degree of elongation determined by X-rays.

(iii) When the models were ordered on the basis of their lowest *R*-factors, this resulted in the identification of 10 best-fit models for each of the four IgG4 concentrations. These best-fit models are found as a single cluster (green in Supplementary Figure 2), suggesting that a single best-fit family of structures has been identified. The *R*-factor values were low at 2% compared to other modelling fits [24]. Both the R_G and $R_{XS\text{-}1}$ values for these 10 best-fit models are within acceptable error of the experimental values (Table 1). In particular, the model for 0.3 mg/ml showed a slightly lower $R_{XS\text{-}1}$ value and a more reduced $R_{XS\text{-}2}$ value when compared with those for the other three concentrations (Table 1).

The outcome of the modelling analyses in terms of best-fit models is summarised in Figure 6. Good curve fits were obtained in all four cases, both for the experimental *I(Q)* curves and the *P(r)* curves shown as insets. The four models in Figure 6 display a range of Fab conformations compared to the Fc region. The models do not indicate a simple explanation for the concentration dependence of the two peaks in the *P(r)* curves. The previous modelling of IgA1, IgA2 and IgD showed that similar T-shaped or Y-shaped structures resulted in *P(r)* curves with either one or two peaks. Accordingly, the distribution of the distances *d1*, *d2* and *d3* between the centres of the Fab and Fc regions in the 100 best fit IgG4 models was investigated (Supplementary Figure 3(a-c)). Comparisons of *d1*, *d2* and *d3* showed that only a limited range of distances fitted the data, mostly in the upper right corners in Supplementary Figure 3(a-c). This showed that only the more extended hinges in IgG4 fitted the X-ray data best.

Even though much scatter is present in Supplementary Figure 3, the distribution of *d1* vs. *d3* distances explained the observed *P(r)* differences with concentration. The ten best-fit models at 0.3 mg/ml (dark blue) cluster around *d3* = 6 nm and *d1* = 7 nm. The three higher concentrations show two clusters of best-fit structures at either *d3* = 8 nm and *d1* = 5 nm, or at *d3* = 5 nm and *d1* = 8 nm. Because the two Fab fragments are equivalent in the IgG4 structure, the two clusters correspond in fact to the same IgG4 structure, and show that the *d3* distances correspond to a more extended structure at higher concentration compared to that at 0.3 mg/ml. The ten best-fit structures at 1.3 mg/ml and 0.3 mg/ml were examined after their Fc regions were superimposed (PDB codes 3m7x and 3m80) with a viewer such as RASMOL (http://www.openrasmol.org/). Although the Fab positions vary, the Fab regions appear more separated at 1.3 mg/ml than at 0.3 mg/ml, which corresponds to the increase of *d3* to 8 nm. The occurrence of two clusters is best explained by the asymmetry of the Fab and Fc regions within the IgG4 structure at higher concentration, much as seen in the crystal structure of human IgG1. One Fab region cannot approach the near side of the Fc region unless the other

Fab region is moved away. This best-fit solution structure for IgG4 is however notably different from that for the IgG1 crystal structure, for which the *d1*, *d2* and *d3* distances are denoted by a black cross in Supplementary Figure 3.

Sedimentation coefficient modelling for human IgG4

The sedimentation coefficient $s_{20,w}$ value of the 10 best-fit X-ray scattering IgG4 models were calculated for comparison with the experimental values of 6.44 S (Figure 3). The calculated $s_{20,w}$ values for the 10 models for each of the four concentrations ranged between 6.61 S to 6.77 S using HYDRO (Table 1). The corresponding four sets of $s_{20,w}$ values using HYDROPRO ranged between 6.39 S to 6.60 S (Table 1). Given that the calculations are generally accurate to within ± 0.21 S [24], both sets of $s_{20,w}$ values agree well with the experimental value of 6.44 S. In previous applications of HYDRO and HYDROPRO to antibody structures, large discrepancies had occasionally been observed with the use of HYDRO, but not with HYDROPRO [49]. This discrepancy was not observed here, showing that the independent modelling of each of the X-ray and $s_{20,w}$ data sets have resulted in a self-consistent structural outcome.

DISCUSSION

IgG4 structure and function

Our IgG4 analyses resulted in the determination of an asymmetric antibody conformation in solution that revealed new insight into function (Figure 7). The two Fab regions partially mask the Fc region in IgG4. This structure has implications for (i) C1q binding to IgG4, which is important for complement activation; (ii) the self-association of IgG4, which may be relevant for rheumatoid factor-like IgG self-binding; and (iii) the formation of bi-specific IgG4 molecules.

C1q binding to IgG activates the classical pathway of complement. Unlike IgG1 which possesses three extra residues in the upper hinge, but which is otherwise identical to IgG4, IgG4 does not activate complement through its C1q binding site at the top of the C_H2 domain in the Fc region. Glu335, Lys337 and Lys339 are the core residues for C1q binding (Figure 7(f)), and appear in both the IgG4 and IgG1 sequences (Supplementary Figure 1(f)) [51]. The difference in C1q binding between IgG4 and IgG1 is clarified by our models. For IgG4, molecular views of each of the four sets of ten superimposed best-fit IgG4 models (PDB codes 3m7x, 3m7y, 3m7z and 3m80) shows that the Fab regions are positioned at the top of the Fc region and along one Fc face, but leaves the other Fc face exposed (Figure 7(d,e)). Glu335, Lys337 and Lys339 are located above and below the Fc region as viewed (Figure 7(f)). It is not possible for the C1q head to interact with the Fc region in IgG4 without encountering steric clash with the Fab regions that are close to the Fc region. This analysis was tested using solvent-accessible surface calculations by the Lee-Richards method [52]. The use of a sphere of radius 0.14 nm to represent a water molecule showed that Glu335, Lys337 and Lys339 were 80-90%, 60% and 60% solvent accessible respectively in the four best fit IgG4 models (Table 1). The use of spheres with five radii between 0.5-4.0 nm to represent the C1q head of approximate radius 3 nm (Figure 7(f)) showed that the surface accessibility of these three residues within IgG4 was reduced to 0% even with a sphere of radius 1 nm. For IgG1, the single view of the IgG1 crystal structure (PDB code 1hzh) shows that both Fab regions are positioned above and below the Fc region (Figure 7(f)), where they now offer no hindrance of C1q access to the Fc region [53].

The self-binding of human IgG1 and IgG4 is relevant in the context of auto-antibodies associated with rheumatoid arthritis. In the present study, intact IgG4 at 2 – 11 μM in solution does not interact with itself. Interestingly, when IgG4 is immobilised on a solid support, this self-associates with IgG4 in the solution phase [54]. This self-association presumably occurs because IgG4 immobilisation makes the Fc region more accessible because the Fab regions have become partially displaced. If IgG4 Fc is immobilised on a sensor surface, a small amount of Fc self-association is detected with a dissociation constant K_D of 1 μM [54]. This self-association is inferred to occur because the Fab regions are not present to mask the immobilised Fc regions. These comparisons support the view that the Fc regions in IgG4 at 2 – 11 μM in solution are masked by the Fab regions.

In addition, even though the overall IgG4 shape is unaffected by concentration, the observed alterations in both Fab-Fc hinge lengths and Fab-Fab separations within IgG4 with concentration may be related to the observation of bispecificity in IgG4. The ready exchange between monospecific and bispecific forms of IgG4 in the reducing environment of red blood cells may be facilitated by molecular crowding at the hinge region in IgG4 caused by the proximity between the Fab and Fc regions [55]. This exchange process also involves the C_H3 domains which also make inter-heavy-chain contacts [55]. When hinge crowding is

supplemented by the reduction of disulphide bridges between the two IgG4 heavy chains, steric crowding at the hinge would facilitate heavy chain exchange between different IgG4 molecules. The transient formation of half-molecules of IgG4 leads to the observed inability of IgG4 antibody to cross-link identical antigens through bivalent binding, as well as the existence of bispecific IgG4 molecules.

Hinge structure of IgG4

The X-ray modelling showed that the IgG4 hinge possesses a mostly extended structure in solution, and that the Fab and Fc regions show modest but detectable alterations with concentration. This asymmetric solution structure for IgG4 is attributed to its hinge sequence. Molecular views show that the hinge is not sufficiently long to permit the three Fab and Fc regions in IgG4 to exhibit unrestricted freedom of conformational rearrangement about the hinge. The upper hinge in IgG4 is only seven residues long, compared to the ten residues in the upper hinge of IgG1, and IgG4 possesses the shortest middle hinge of the four human IgG subclasses [2]. It is not surprising that the IgG4 upper hinge is structurally extended in order to be able to accommodate its Fab and Fc regions. The length of the upper hinge was defined by the α-carbon positions of the flanking residues Arg231 and Pro244. The maximum possible length for ten peptide bonds in an extended conformation is 3.8 nm. The ten best-fit structures from the four IgG4 concentrations gave hinge lengths that increased from 2.8 nm to 3.6 nm with dilution (Table 2). This increase is accompanied by a decreased separation between the Fab regions and an increased separation between the Fab-Fc regions with dilution (Figure 7). In comparison, the corresponding distances between the α-carbons of Lys222 and Pro240 (PDB 1hzh numbering) in the IgG1 upper hinge is 2.6 nm and 2.7 nm. The shorter length of the IgG1 upper hinge may be the consequence of its extra three residues that facilitates greater conformational possibilities between the Fab and Fc regions (Supplementary Figure 1(e)).

The solution conformation of IgG4 can be compared with IgG4 structures previously reported by electron microscopy, using angles measured between the Fab and Fc regions. In our IgG4 models, the mean Fab-Fab angle ranged between 76° to 105° with standard deviations of up to 47° (Table 2). Two different sets of Fab-Fc angles resulted because of the asymmetric IgG4 solution models, and these ranged between 120-139 ° and 64-90°. By electron microscopy, the mean Fab-Fab angle in IgG4 was 128° ± 39° and the mean Fab-Fc angle was 98° ± 25°, and similar values were reported for IgG1, IgG2 and IgG3 [22]. A more recent study reported mean Fab-Fab angles of 96° ± 26° and 99° ± 17° for a murine MMA 383 antibody [56]. It is deduced that the electron microscopy angles are in good accord with those from the scattering modelling of IgG4.

The concentration dependence of the IgG4 structure corresponds to an internal structural rearrangement of the Fab and Fc regions. No change in overall shape is observed from the $s_{20,w}$ and R_G values, and IgG4 dissociation into two halves is ruled out from the *c(s)* analyses. There are two possible explanations for this based on fast non-binding interactions. Firestly, it is possible that greater diffusion-collision rates between IgG4 molecules at 1.3 mg/ml may alter the internal arrangement of the Fab and Fc regions within IgG4 compared to that at 0.3 mg/ml. At 1.3 mg/ml, the average separation between IgG4 molecules will be about 58 nm. At 0.3 mg/ml, this average separation will be reduced to about 94 nm. These separations are comparable with the 17 nm size of IgG4 molecules (Table 1). Alternatively, given the presence of 272 charged residues (21%) in a total of 1315 residues in IgG4, long range electrostatic fields between IgG4 molecules at higher concentration may influence the arrangement of Fab and Fc regions within IgG4. Physiologically, the conformation at 1.3

mg/ml is more likely to be relevant, given that serum proteins exist in a crowded environment at 80 mg/ml in blood, and also during conditions of bioprocessing during which reagent concentrations of as high as 20 mg/ml will be encountered [5,6].

The present study represents advances in comparison to earlier similar studies. Previous X-ray scattering experiments at synchrotrons often employed a minimum concentration of 2 mg/ml [19,21]. Here, excellent signal-noise ratios were attainable even at 0.3 mg/ml (Table 1), this being attributed to improvements in detector technologies. X-ray scattering can be limited by aggregated material that may increase R_G values by as much as 5-10% and perturb the modelling [18,20]. Here, the absence of aggregates was confirmed by the independent use of ultracentrifugation *c(s)* analyses and the good agreement between the X-ray and $s_{20,w}$ modelling. A limitation of earlier studies is the use of simple shape models to model the antibody structure [18-21]. Here, the use of atomic starting models for IgG4 to result in families of best-fit structures resulted in more convincing molecular insight into the solution data.

Stability of therapeutic IgG4

In terms of the industrial bio-processing of antibodies, the clarification of the solution conformation of IgG4 and the relative movement of the Fab and Fc domains within this may be important for its aggregation and surface adhesion effects during its manufacture and storage as biopharmaceuticals. These alterations may modulate their susceptibility to interactions with other proteins or container surfaces. Our IgG4 results will enable us to examine the impact of low pH conditions on IgG4 during its elution from Protein A or Protein G resins during large scale chromatography. This key step is frequently implicated in the loss of antibody to aggregation with nearly half of this class of medicine found to have such issues [57].

AUTHOR CONTRIBUTION

Yuki Abe designed and performed experiments, analysed data and wrote the manuscript; Jayesh Gor designed and performed experiments; Daniel Bracewell, Stephen Perkins and Paul Dalby designed the study, analysed data and wrote the manuscript.

ACKNOWLEDGEMENTS

We thank the Innovative Manufacturing Research Centre in Bioprocessing at UCL for grant support, the Biotechnology and Biological Sciences Research Council, the Henry Smith Charity and the Mercer Fund of the Fight For Sight Charity for equipment support, Dr J. Davies (Lonza Biologics) for generously providing human IgG4, and Dr Alexandra Bonner and Dr Azubuike I. Okemefuna for excellent computational support.

REFERENCES

1 Hamilton, R. G. (2001) The human IgG subclasses. Calbiochem Corporation.

2 Brekke, O. H., Michaelson, T. E. and Sandlie, I. (1995) The structural requirements for complement activation by IgG: does it hinge on the hinge? Immunol. Today, **16**, 85-90.

3 Aalberse, R. C. and Schuurman, J. (2002) IgG4 breaking the rules. Immunology, **105**, 9-19.

4 Rispens, T., den Bleker, T. H. and Aslberse, R. C. (2010) Hybrid IgG4/IgG4 Fc antibodies form upon 'Fab-arm' exchange as demonstrated by SDS-PAGE or size-exclusion chromatography. Molec. Immunol. In press

5 Wang, W., Singh, S., Zeng, D. L., King, K. and Nema, S. (2007) Antibody structure, instability and formulation. J. Pharm. Sci. **96**, 1-26.

6 Wang, X., Das, T. K., Singh, S. K. and Kumar, S. (2009) Potential aggregation prone regions in biotherapeutics: A survey of commercial monoclonal antibodies. mAbs, **1**, 254-267.

7 Bonner, A., Furtado, P. B., Almogren, A., Kerr, M. A. and Perkins, S. J. (2008) Implications of the near-planar solution structure of human myeloma dimeric IgA1 for mucosal immunity and IgA nephropathy. J. Immunol. **180**, 1008-1018.

8 Bonner, A., Almogren, A., Furtado, P. B., Kerr, M. A. and Perkins, S. J. (2009) Location of secretory component on the Fc edge of dimeric IgA1 reveals insight into the role of secretory IgA1 in mucosal immunity. Mucosal Immunology (Nature Publishing Group), **2**, 74-84.

9 Saphire, E. O., Parren, P. W., Pantophlet, R., Zwick, M. B., Morris, G. M., Rudd, P. M., Dwek, R. A., Stanfield, R. L., Burton, D. R. and Wilson, I. A. (2001) Crystal structure of a neutralizing human IgG against HIV-1: a template for vaccine design. Science, **293**, 1155-1159.

10 Saphire, E. O., Stanfield, R. L., Crispin, M. D. M., Parren, P. W. H. I., Rudd, P. M., Dwek, R. A., Burton, D. R. and Wilson, I. A. (2002) Contrasting IgG structures reveal extreme asymmetry and flexibility. J. Mol. Biol. **319**, 9-18.

11 Harris, L. J., Larson, S. B., Hasel, K. W. and McPherson, A. (1997) Refined structure of an intact IgG2a monoclonal antibody Biochemistry, **36**, 1581-1597.

12 Harris, L. J., Skaletsky, E. and McPherson, A. (1998) Crystallographic structure of an intact IgG1 monoclonal antibody. J. Mol. Biol. **275**, 861-872.

13 Cromwell, M. E. M., Hilario, E. and Jacobson, F. (2006) Protein aggregation and bioprocessing. The AAPS Journal **8**, E572-E579.

14 Sukumar, M., Doyle, B. L., Combs, J. L. and Pekar, A. H. (2004) Opalescent appearance of an IgG1 antibody at high concentrations and its relationship to noncovalent association. Pharmac. Res. **21**, 1087-1093.

15 Manning, M. C., Chou, D. K., Murphy, B. M., Payne, R. W. and Katayama, D. S. (2010) Stability of Protein Pharmaceuticals: An Update. Pharmac. Res. **27**, 544-575.

16 Biddlecombe, J. G., Smith, G., Uddin, S., Mulot, S., Spencer, D., Gee, C., Fish, B. C. and Bracewell, D. G. (2009) Factors Influencing Antibody Stability at Solid–Liquid Interfaces in a High Shear Environment. Biotechnol. Prog. **25**, 1499–1507.

17 Mayans, M. O., Coadwell, W. J., Beale, D., Symons, D. and Perkins, S. J. (1995) Demonstration by pulsed neutron scattering that the arrangement of the Fab and Fc fragments in the overall structures of bovine IgG1 and IgG2 in solution is similar. Biochem. J. **311,** 283-291.

18 Gregory, L., Davis, K. G., Sheth, B., Boyd, J., Jefferis, R., Nave, C. and Burton, D. R. (1987) The solution conformations of the subclasses of human IgG deduced from

sedimentation and small angle X-ray scattering studies. Molec. Immunol. **24**, 821-829.

19 Longman, E., Kreusel, K., Tendler, S. B., Fiebrig, I., King, K., Adair, J., O'Shea, P., Ortega, A., Garcia de la, T. J. and Harding, S. E. (2003) Estimating domain orientation of two human antibody IgG4 chimeras by crystallohydrodynamics. Eur. Biophys. J. **32**, 503-510.

20 Lu, Y., Harding, S. E., Michaelsen, T. E., Longman, E., Davis, K. G., Ortega, A., Grossmann, J. G., Sandlie, I. and Garcia de la Torre, J. (2007) Solution conformation of wild-type and mutant IgG3 and IgG4 immunoglobulins using crystallohydrodynamics: possible implications for complement activation. Biophys. J. **93**, 3733-3744.

21 Lu, Y., Harding, S. E., Rowe, A. J., Davis, K. G., Fish, B., Varley, P., Gee, C. and Mulot, S. (2008) The effect of a point mutation on the stability of IgG4 as monitored by analytical ultracentrifugation. J. Pharmac. Sci. **97**, 960-969.

22 Roux, K. H., Strelets, L. and Michaelsen, T. E. (1997) Flexibility of human IgG subclasses. J. Immunol. **159**, 3372-3382.

23 Perkins, S. J. and Bonner, A. (2008) Structure determinations of human and chimaeric antibodies by solution scattering and constrained molecular modelling. Biochem. Soc. Transact. **36**, 37-42.

24 Perkins, S. J., Okemefuna, A. I., Nan, R., Li, K. and Bonner, A. (2009) Constrained solution scattering modelling of human antibodies and complement proteins reveals novel biological insights. J. Roy. Soc. Interface. **6**, S679-S696.

25 Perkins, S. J., Nealis, A. S., Sutton, B. J. and Feinstein, A. (1991) The solution structure of human and mouse immunoglobulin IgM by synchrotron X-ray scattering and molecular graphics modelling: a possible mechanism for complement activation. J. Mol. Biol. **221**, 1345-1366.

26 Boehm, M. K., Woof, J. M., Kerr, M. A. and Perkins, S. J. (1999) The Fab and Fc fragments of IgA1 exhibit a different arrangement from that in IgG: a study by X-ray and neutron solution scattering and homology modelling. J. Mol. Biol. **286**, 1421-1447.

27 Aslam, M., Guthridge, J. M., Hack, B. K., Quigg, R. J., Holers, V. M. and Perkins, S. J. (2003) The extended multidomain solution structures of the complement protein Crry and its chimeric conjugate Crry-Ig by scattering, analytical ultracentrifugation and constrained modelling: implications for function and therapy. J. Mol. Biol. **329**, 525-550.

28 Furtado, P. B., Whitty, P. W., Robertson, A., Eaton, J. T., Almogren, A., Kerr, M. A., Woof, J. M. and Perkins, S.J. (2004) Solution structure determination of monomeric human IgA2 by X-ray and neutron scattering, analytical ultracentrifugation and constrained modelling: a comparison with monomeric human IgA1. J. Mol Biol. **338,** 921-941.

29 Sun, Z., Almogren, A., Furtado, P. B., Chowdhury, B., Kerr, M. A. and Perkins, S. J. (2005) Semi-extended solution structure of human myeloma immunoglobulin D determined by constrained X-ray scattering. J. Mol. Biol. **353**, 155-173.

30 Perkins, S. J., Okemefuna, A. I., Fernando, A. N., Bonner, A., Gilbert, H. E. and Furtado, P. B. (2008) X-ray and neutron scattering data and their constrained molecular modelling. Meth. Cell Biol. **84**, 375-423.

31 Okemefuna, A. I., Nan, R., Gor, J. and Perkins, S. J. (2009) Electrostatic interactions contribute to the folded-back conformation of wild-type human Factor H. J. Mol. Biol. **391**, 98-118.

32 Cole, J. L., Lary, J. W., Moody, T. P. and Laue, T. M. (2008) Analytical ultracentrifugation: sedimentation velocity and sedimentation equilibrium. Meth. Cell Biol. **84**, 143-211.

33 Brady, R. L., Hubbard, R. E., King, D. J., Low, D. C., Roberts, S. M. and Todd, R. J. (1991) Crystallization and preliminary X-ray diffraction study of a chimaeric Fab' fragment of antibody binding tumour cells. J. Mol. Biol. **219**, 603-604.

34 Perkins, S. J. (1986) Protein volumes and hydration effects: the calculation of partial specific volumes, neutron scattering matchpoints and 280 nm absorption coefficients for proteins and glycoproteins from amino acid sequences. Eur. J. Biochem. **157**, 169-180.

35 Schuck, P. (1998) Sedimentation analysis of non-interacting and self-associating solutes using numerical solutions to the Lamm equation. Biophys. J. **75**, 1503-1512.

36 Schuck, P. (2000) Size-distribution analysis of macromolecules by sedimentation velocity ultracentrifugation and Lamm equation modeling. Biophys J. **78**, 1606-1619.

37 Narayanan, T., Diat, O. and Bosecke, P. (2001) SAXS and USAXS on the high brilliance beamline at the ESRF. Nucl. Instrum. Methods Phys. Res. A, **467-468**, 1005-1009.

38 Li, K., Okemefuna, A. I., Gor, J., Hannan, J. P., Asokan, R., Holers, V. M. and Perkins, S. J. (2008) Solution structure of the complex formed between human complement C3d and full length complement receptor Type 2. J. Mol. Biol. **384**, 137-150.

39 Gilbert, H. E., Eaton, J. T., Hannan, J. P., Holers, V. M. and Perkins, S. J. (2005) Solution structure of the complex between CR2 SCR 1-2 and C3d of human complement: an X-ray scattering and sedimentation modelling study. J. Mol. Biol. **346**, 859-873.

40 Glatter, O. and Kratky, O. (1982) Editors of Small-angle X-ray scattering. Academic Press, New York.

41 Pilz, I., Kratky, O., Licht, A. and Sela, M. (1973) Shape and volume of anti-poly(D-alanyl) antibodies in the presence and absence of tetra-D-alanine as followed by small-angle X-ray scattering. Biochemistry, **12**, 4998-5005.

42 Semenyuk, A. V. and Svergun, D. I. (1991) GNOM - a program package for small-angle scattering data-processing. J. Appl. Crystallogr. **24,** 537-540.

43 Arnold K., Bordoli L., Kopp J. and Schwede T. (2006) The SWISS-MODEL Workspace: A web-based environment for protein structure homology modelling. Bioinformatics, **22**,195-201.

44 Perkins, S. J. and Weiss, H. (1983) Low resolution structural studies of mitochondrial ubiquinol-cytochrome c reductase in detergent solutions by neutron scattering. J. Mol. Biol. **168**, 847-866.

45 Ashton, A. W., Boehm, M. K., Gallimore, J. R., Pepys, M. B. and Perkins, S. J. (1997) Pentameric and decameric structures in solution of the serum amyloid P component by X-ray and neutron scattering and molecular modelling analyses. J. Mol. Biol. **272**, 408-422.

46 Perkins, S. J. (2001) X-ray and neutron scattering analyses of hydration shells: a molecular interpretation based on sequence predictions and modelling fits. Biophys. Chem. **93**, 129-139.

47 Garcia de la Torre, J., Navarro, S., Martinez, M. C. L., Diaz, F. G. and Cascales, J. L. (1994) HYDRO: A computer program for the prediction of hydrodynamic properties of macromolecules. Biophys. J. **67**, 530–531.

48 Garcia de la Torre, J., Huertas, M. L. and Carrasco, B. (2000) Calculation of hydrodynamic properties of globular proteins from their atomic-level structure. Biophys. J. **78**, 719-730.

49 Almogren, A., Furtado, P. B., Sun, Z., Perkins, S. J. and Kerr, M. A. (2006) Purification, properties and extended solution structure of the complex formed between human immunoglobulin A1 and human serum albumin by scattering and ultracentrifugation. J. Mol. Biol. **356**, 413-431.

50 Bloom, J. W., Madanat, M. S., Marriott, D., Wong, T. and Chan, S.-Y. (1997) Intrachain disulphide bond in the core hinge region of human IgG4. Protein Science, **6**, 407-415.

51 Harris, L. J., Larson, S. B. and McPherson, A. (1999) Comparison of intact antibody structures and the implications for effector function. Adv. Immunol. **72**, 191-208.

52. Lee, B. and Richards, F. M. (1971) The interpretation of protein structures: estimation of static accessibility. J. Mol. Biol. **55**, 379-400.

53 Gaboriaud, C., Juanhuix, J., Gruez, A., Lacroix, M., Darnault, C., Pignol, D., Verger, D, Fontecilla-Camps, J. C. and Arlaud, G. J. (2003) The crystal structure of the globular head of complement protein C1q provides a basis for its versatile recognition properties. J. Biol. Chem. **278**, 46974-46982.

54. Rispens, T., Heer, P. O., Vermeulen, E., Schuurman, J. van der Neut Kolfschoten, M. and Aalberse, R. C. (2009) Human IgG4 Binds to IgG4 and conformationally altered IgG1 via Fc-Fc interactions. J. Immunol. **182**, 4275-4281.

55 van der Neut Kolfschoten, M., Schuurman, J., Losen, M., Bleeker, W. K., Martínez-Martínez, P., Vermeulen, E., den Bleker, T. H., Wiegman, L., Vink, T., Aarden, L. A., De Baets, M. H., van de Winkel, J. G. J., Aalberse, R. C. and Parren, P. W. H. I. (2007) Anti-inflammatory activity of human IgG4 antibodies by dynamic Fab arm exchange. Science **317**, 1554-1557.

56 Taschner, N., Műller, S. A., Alumella, V. R., Goldie, K. N., Drake, A. F., Aebi, U. and Arvinte, T. (2001) Modulation of antigenicity related to changes in antibody flexibility upon lyophilisation. J. Mol. Biol. **310**, 169-179.

57 Shukla, A. A., Hubbard, B., Tressel, T., Guhan, S. and Low, D. (2007) Downstream processing of monoclonal antibodies: application of platform approaches. J. Chromatogr. B. **848**, 28-39.

Table 1. X-ray scattering and sedimentation coefficient data for IgG4 and their modelling

	R_G (nm)	R_{XS-1} (nm)	R_{XS-2} (nm)	D_{max} (nm)	R factor (%)	$s^0_{20,w}$ (S)
A. Experimental data						
IgG4 (1.30 mg/ml)	4.98 ± 0.08 ; 5.08 ± 0.12 [a]	2.55 ± 0.03	1.41 ± 0.02	17		6.44 [b]
IgG4 (0.98 mg/ml)	5.00 ± 0.09; 5.03 [a]	2.56 ± 0.01	1.44 ± 0.02	17		6.44 [b]
IgG4 (0.65 mg/ml)	5.03 ± 0.03; 5.04 [a]	2.57 ± 0.03	1.46 ± 0.06	17		n.a.
IgG4 (0.30 mg/ml)	4.92 ± 0.25; 4.96 [a]	2.55 ± 0.08	1.26 ± 0.05	17		n.a.
B. Modelling of IgG4 [c]						
IgG4 (1.30 mg/ml)	4.87	2.61	1.35	17 [d]	2.0	6.69, 6.46 [e]
IgG4 (0.98 mg/ml)	4.93	2.55	1.49	17 [d]	2.0	6.51, 6.67 [e]
IgG4 (0.65 mg/ml)	4.84	2.60	1.46	17 [d]	2.3	6.71, 6.54 [e]
IgG4 (0.30 mg/ml)	4.91	2.54	1.22	17 [d]	3.8	6.65, 6.41 [e]

[a] The first value is from the Guinier R_G analyses (Figure 3(a) and the second one is from the GNOM $P(r)$ analyses (Figure 4(a)).

[b] The values were measured at 1.6 mg/ml and 0.8 mg/ml

[c] The full description of the modelling is reported in Table 1 of the Supplementary Material.

n.a. not available

[d] From Figure 6(a-d). [e] The first value corresponds to that from HYDRO; the second from HYDROPRO.

TABLE 2. Summary of each set of ten IgG4 best fit models

	Mean upper hinge length (nm)	Fab-Fab angle (°)	Fab-Fc angle (°)	Fab-Fc angle (°)
IgG4 (1.30 mg/ml)	2.7 ± 0.2	104 ± 43	139 ± 20	90 ± 32
IgG4 (0.98 mg/ml)	3.5 ± 0.3	96 ± 47	136 ± 21	71 ± 63
IgG4 (0.65 mg/ml)	3.1 ± 0.5	76 ± 39	120 ± 18	74 ± 64
IgG4 (0.30 mg/ml)	3.6 ± 0.1	105 ± 43	137 ± 24	64 ± 55

FIGURE LEGENDS

Figure 1. Domain diagram of the human-mouse chimera IgG4 structure. The heavy chains consist of V_H, C_H1, C_H2 and C_H3 domains, and the light chains each comprise a V_L and C_L domain. There are no disulphide bonds between C_H1 and C_L. The heavy chains are connected by two Cys-Cys disulphide bridge bonds at Cys243 and Cys246. There is one N-linked oligosaccharide site at Asn314 on the two C_H2 domains. The hinge region between the Fab and Fc fragments is comprised of 14 residues (KYGPPCPSCPAPEF) between Ser234 and Leu252. Both the Cys243-Cys243 and Cys246-Cys246 bonds are weakened by the Ser245 substitutions.

Figure 2. Purification of IgG4. (a) Elution peak from Superdex 200 gel filtration column, from which fractions 14-19 were pooled. (b) Non-reduced SDS-PAGE analysis of IgG4. The molecular weight markers in the left lane are denoted in kDa, while the right lane corresponds to IgG4. (c) The corresponding reduced SDS-PAGE analysis of IgG4 is shown.

Figure 3. Sedimentation velocity analyses of IgG4. The experimentally-observed sedimentation boundaries at (a) 1.6 mg/ml and (b) 0.8 mg/ml were recorded using a rotor speed of 50,000 r.p.m.. Thirty boundaries (black) are shown out from 150 scans, these being taken at intervals of every fifth scan for reason of clarity, and fitted as shown (white lines). The size distribution analyses *c(s)* revealed single peaks at sedimentation coefficients of 6.44 S in both cases.

Figure 4. Guinier R_G and R_{XS} analyses for IgG4. Data are shown using four different concentrations of IgG4 (from top to bottom, 1.3 mg/ml, 0.98 mg/ml, 0.65 mg/ml and 0.3 mg/ml). The filled circles between the arrowed data points represent the $Q.R_G$ and $Q.R_{XS}$ ranges used to determine the R_G and R_{XS} values. The Q range used for R_G values is 0.7-1.4 nm^{-1} and those for $R_{XS\text{-}1}$ and $R_{XS\text{-}2}$ are 0.8-1.3 nm^{-1} and 0.9-1.4 nm^{-1} respectively.

Figure 5. Distance distribution analyses *P(r)* for IgG4. (a) The concentration dependence of the *P(r)* curves is shown for 1.3 mg/ml, 0.98 mg/ml, 0.65 mg/ml and 0.30 mg/ml, from top to bottom. The peak maxima at *M1* and *M2* are arrowed. The maximum length of IgG4 at 17 nm is denoted by *L*. (b) The concentration dependence of peaks *M1* (○) and *M2* (▲) is shown for repeated measurements at each of the four concentrations studied.

Figure 6. X-ray scattering curve fits for the best fit IgG4 models at four concentrations. The IgG concentrations are (a) 1.3 mg/ml (red); (b) 0.98 mg/ml (green); (c) 0.65 mg/ml (orange); and (d) 0.30 mg/ml (blue). In the left panels, the experimental data are indicated by circles and the calculated best-fit scattering curve is indicated by continuous lines. The insets correspond to the experimental (black) and best-fit modelled (coloured) *P(r)* curves, in which the *M1* and *M2* values from Figure 5 are arrowed. In the right panels, the best-fit IgG4 models are shown, with the Fab regions in blue and the Fc regions in red.

Figure 7. Views of the best-fit IgG4 models at four concentrations. The IgG4 concentrations correspond to (a) 1.3 mg/ml; (b) 0.98 mg/ml and 0.65 mg/ml; (c) 0.30 mg/ml. Two representative views of the best-fit model at each concentration are shown in order to highlight the Fab-Fab and Fab-Fc separations at different concentrations. The distances *d1* between the centres of mass of the Fab regions (yellow spheres) are marked as shown, together with the distances *d3* between one Fab region and the Fc region. In (d, e), the ten best-fit IgG4 structures at 1.3 mg/ml and 0.3 mg/ml are shown superimposed upon their Fc region (blue; top right). In (f), the crystal structure of human IgG1 is shown with its Fc region

also viewed edge-on in a similar orientation. The heterotrimeric C1q globular head is depicted in terms of its A, B and C chains in three colours adjacent to the Fc region of IgG1 for size comparison. The positions of Glu335, Lys337 and Lys339 on each of the IgG1 heavy chains are highlighted as shown (red, orange and orange respectively).

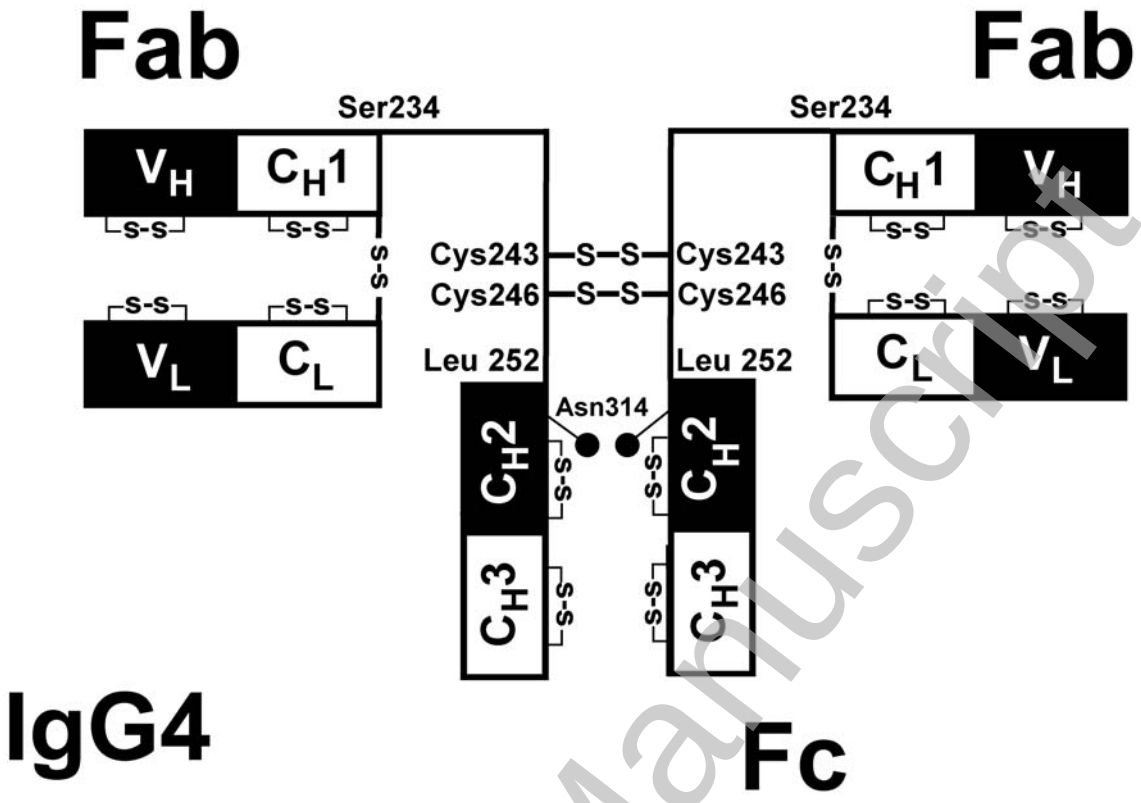

Figure 1

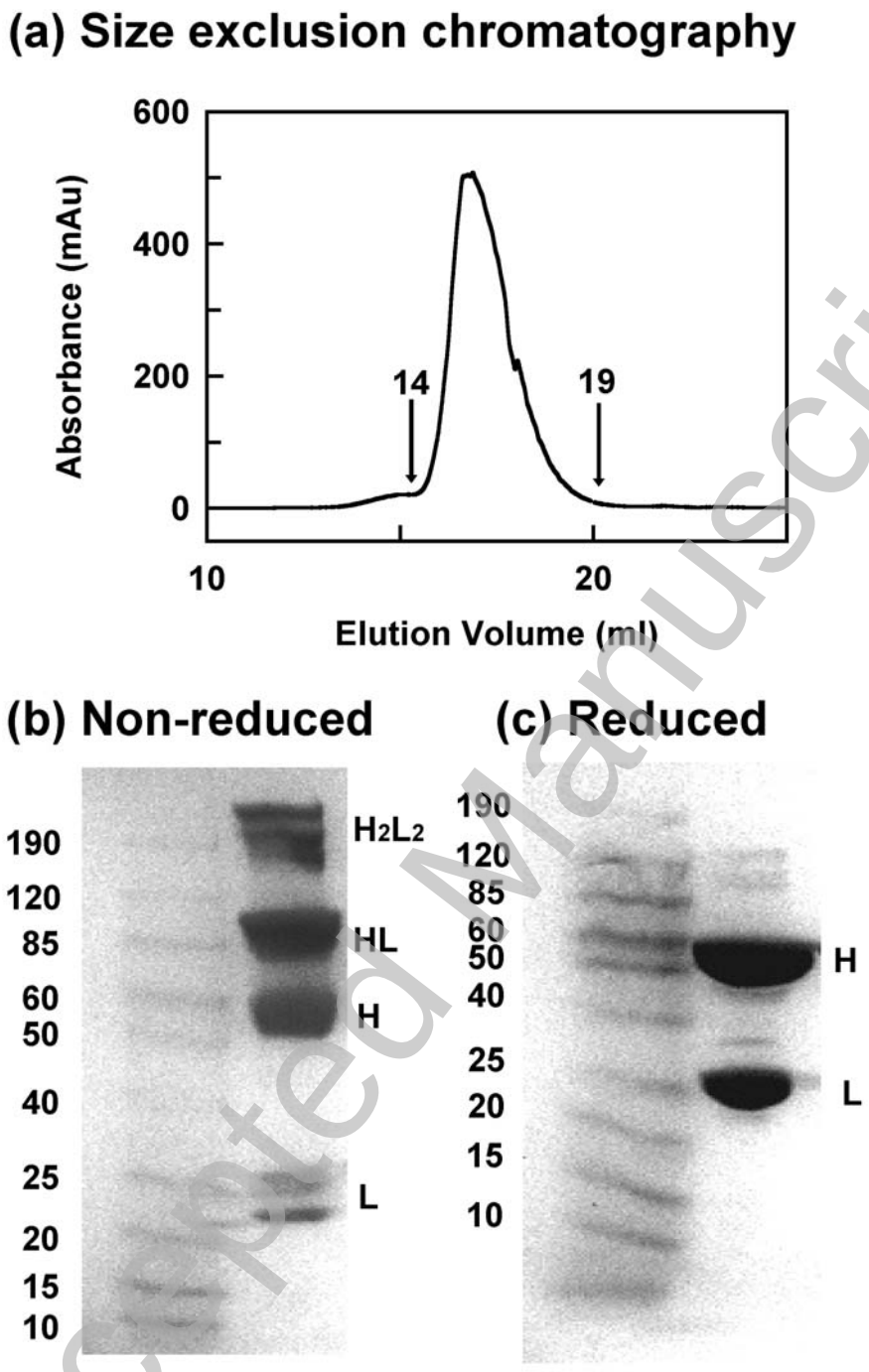

Figure 2

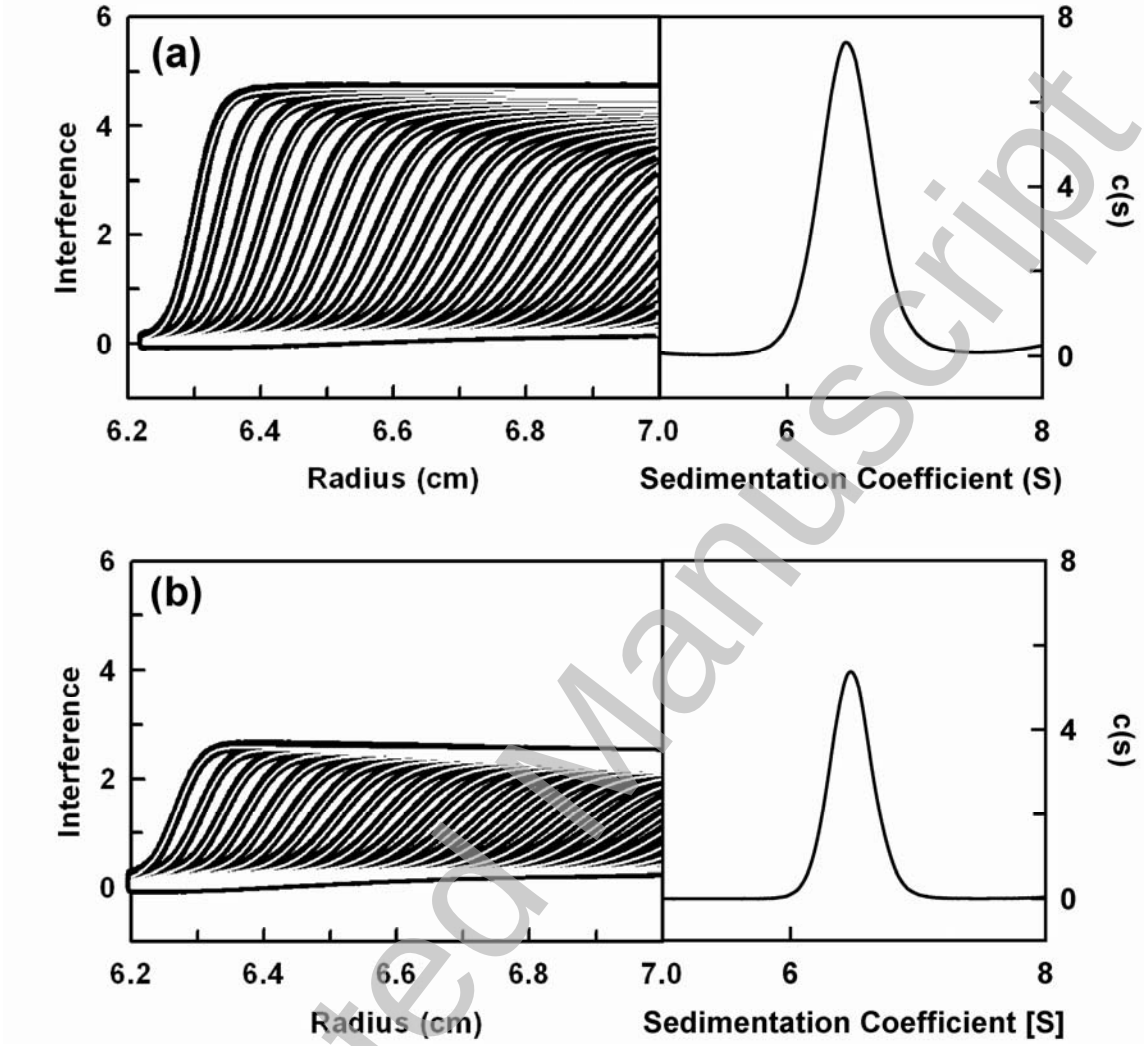

Figure 3

Biochemical Journal Immediate Publication. Published on 20 Aug 2010 as manuscript BJ20100641

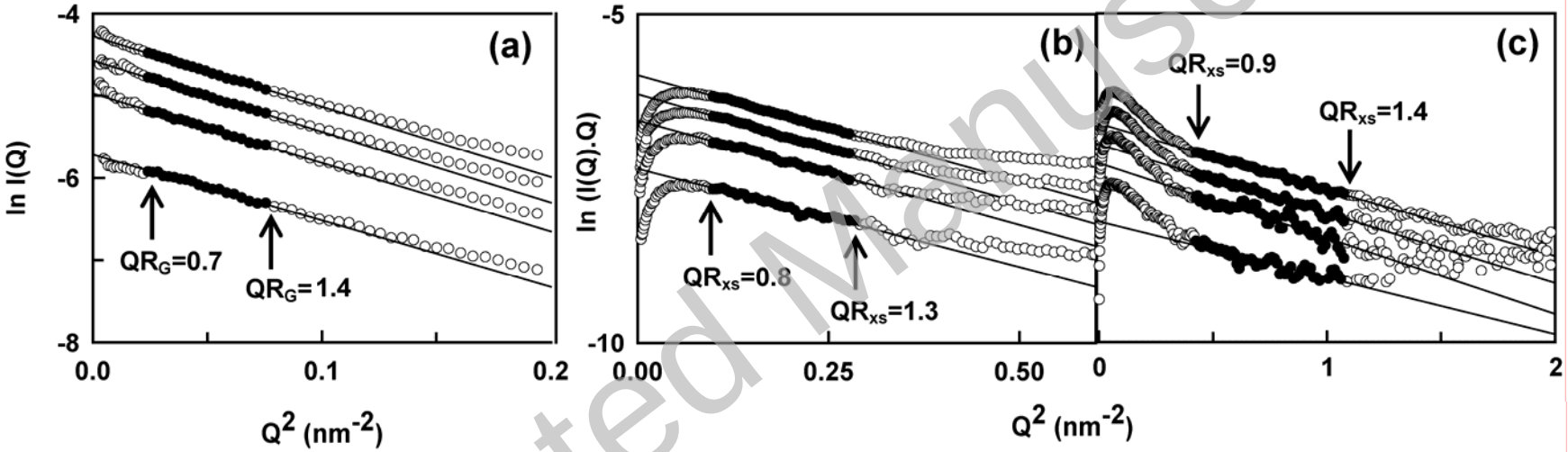

Figure 4

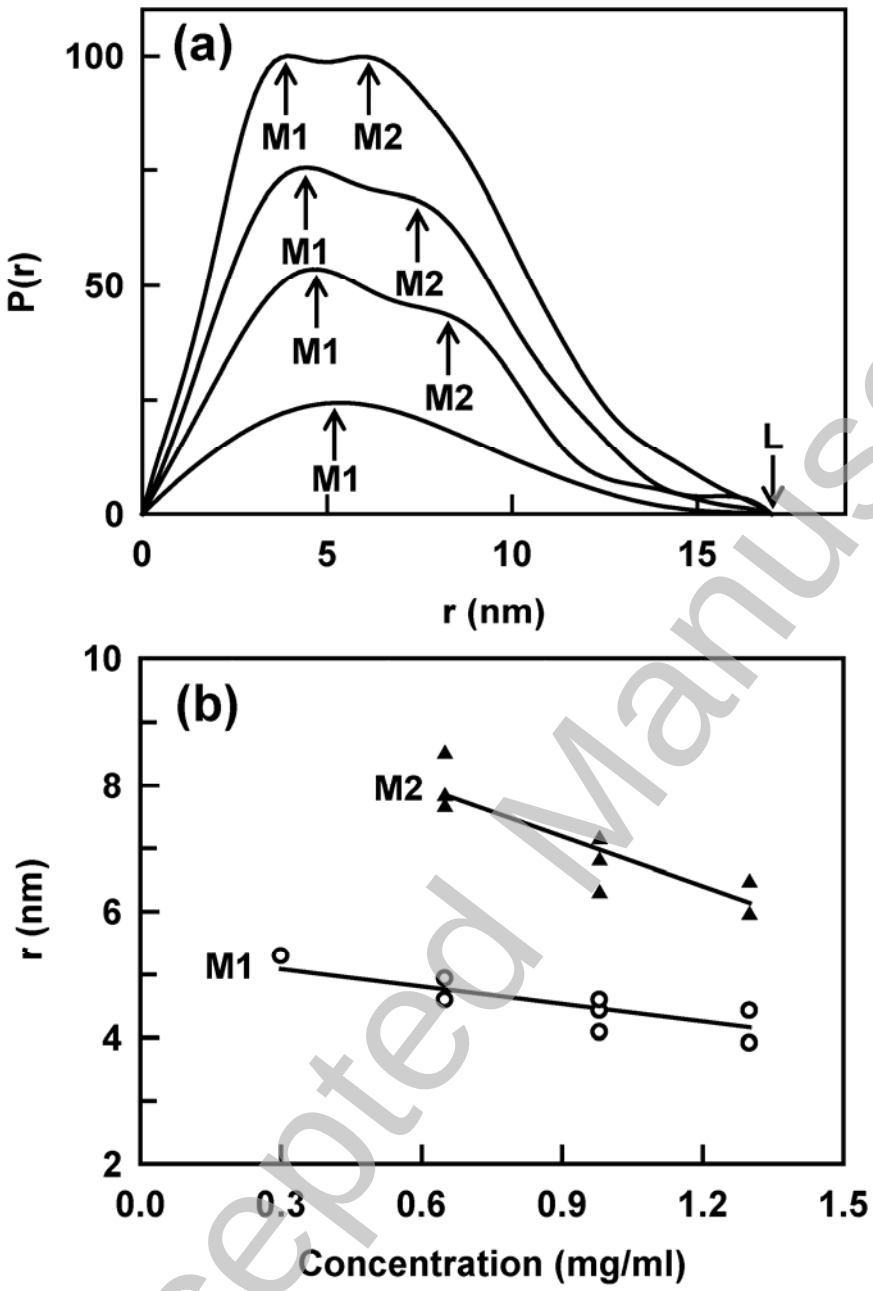

Figure 5

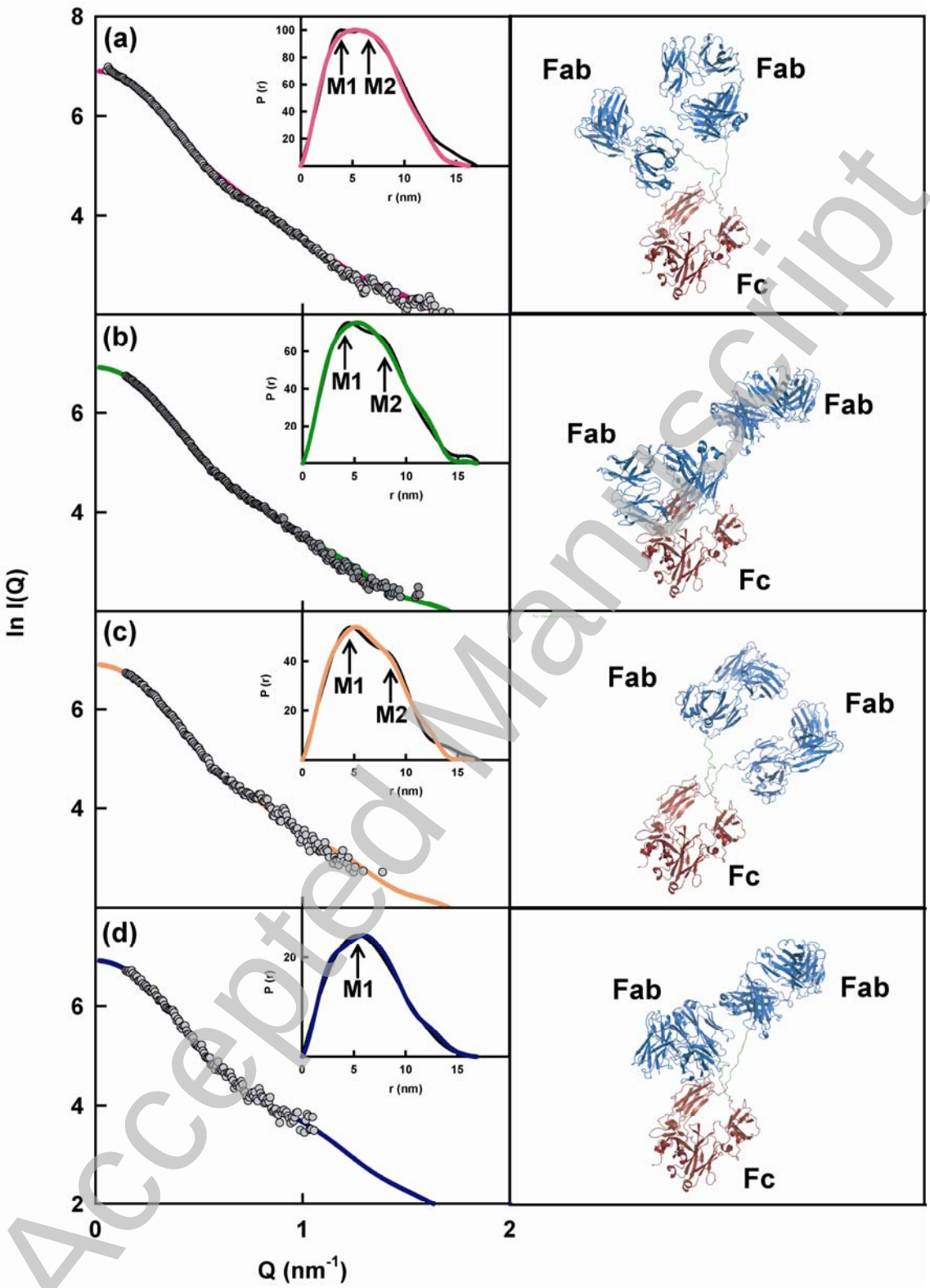

Figure 6

Biochemical Journal Immediate Publication. Published on 20 Aug 2010 as manuscript BJ20100641

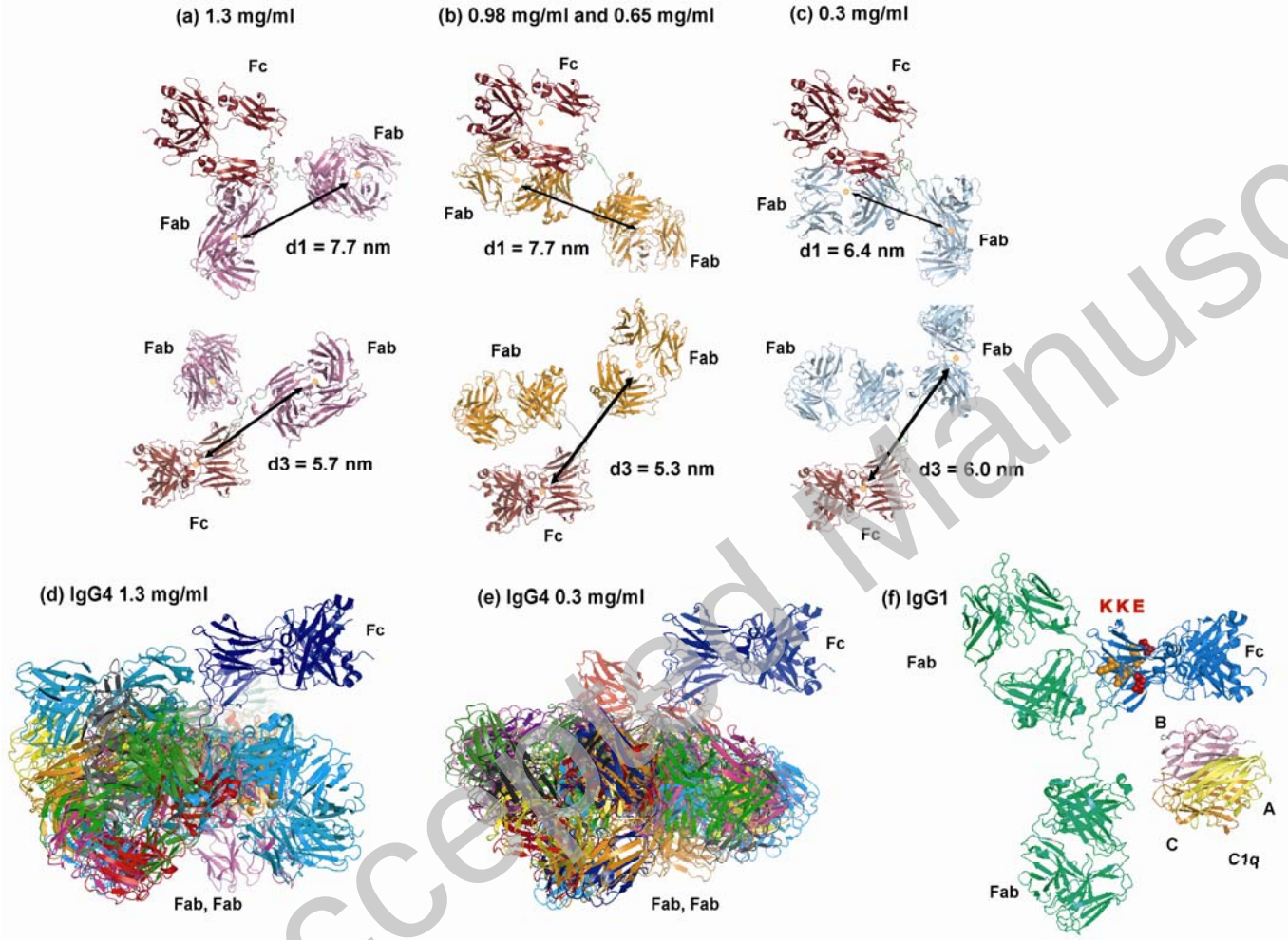

Figure 7